⌘ *Author's Choice*

THE JOURNAL OF BIOLOGICAL CHEMISTRY VOL. 287, NO. 32, pp. 27066–27077, August 3, 2012

Counteracting Effects Operating on Src Homology 2 Domain-containing Protein-tyrosine Phosphatase 2 (SHP2) Function Drive Selection of the Recurrent Y62D and Y63C Substitutions in Noonan Syndrome*◆

Received for publication, February 7, 2012, and in revised form, May 23, 2012 Published, JBC Papers in Press, June 18, 2012, DOI 10.1074/jbc.M112.350231

Simone Martinelli[‡1], Aurelio P. Nardozza[§1], Silvia Delle Vigne[‡], Gilda Sabetta[¶], Paola Torreri[‖], Gianfranco Bocchinfuso[¶], Elisabetta Flex[‡], Serenella Venanzi[‡], Antonio Palleschi[¶], Bruce D. Gelb[‡‡], Gianni Cesareni[§ §§], Lorenzo Stella[¶**], Luisa Castagnoli[§], and Marco Tartaglia[‡2]**

*From the [‡]Dipartimento di Ematologia, Oncologia e Medicina Molecolare and [‖]Centro Nazionale Malattie Rare, Istituto Superiore di Sanità, 00161 Rome, Italy, the [§]Dipartimento di Biologia and [¶]Dipartimento di Scienze e Tecnologie Chimiche, Università di Roma 'Tor Vergata', 00133 Rome, Italy, the **Istituto di Ricovero e Cura a Carattere Scientifico Neuromed, 86077 Pozzilli, IS, Italy, the [‡‡]Child Health and Development Institute, Mount Sinai School of Medicine, New York, New York 10029, and the [§§]IRCCS Fondazione Santa Lucia, 00143 Rome, Italy*

Background: Disease-associated *PTPN11* mutations enhance the function of SHP2 by destabilizing its inactive state or increasing binding to phosphotyrosyl-containing partners.
Results: Amino acid substitutions at codons 62 and 63 have a profound and complex effect on SHP2 structure and function.
Conclusion: A selection-by-function mechanism acting on mutations at those codons implies balancing of counteracting effects operating on the activity of SHP2.
Significance: An unanticipated functional behavior underlies disease-causing weak hypermorphs.

Activating mutations in *PTPN11* cause Noonan syndrome, the most common nonchromosomal disorder affecting development and growth. *PTPN11* encodes SHP2, an Src homology 2 (SH2) domain-containing protein-tyrosine phosphatase that positively modulates RAS function. Here, we characterized functionally all possible amino acid substitutions arising from single-base changes affecting codons 62 and 63 to explore the molecular mechanisms lying behind the largely invariant occurrence of the Y62D and Y63C substitutions recurring in Noonan syndrome. We provide structural and biochemical data indicating that the autoinhibitory interaction between the N-SH2 and protein-tyrosine phosphatase (PTP) domains is perturbed in both mutants as a result of an extensive structural rearrangement of the N-SH2 domain. Most mutations affecting Tyr[63] exerted an unpredicted disrupting effect on the structure of the N-SH2 phosphopeptide-binding cleft mediating the interaction of SHP2 with signaling partners. Among all the amino acid changes affecting that codon, the disease-causing mutation was the only substitution that perturbed the stability of the inactive conformation of SHP2 without severely impairing proper phosphopeptide binding of N-SH2. On the other hand, the disruptive effect of the Y62D change on the autoinhibited conformation of the protein was balanced, in part, by less efficient binding properties of the mutant. Overall, our data demonstrate that the selection-by-function mechanism acting as driving force for *PTPN11* mutations affecting codons 62 and 63 implies balancing of counteracting effects operating on the allosteric control of the function of SHP2.

Germline missense mutations in *PTPN11* occur in ~50% of individuals affected by Noonan syndrome (NS)[3] (1, 2), a relatively common developmental disorder characterized by postnatally reduced growth, facial dysmorphism, webbing of the neck, congenital heart defects and hypertrophic cardiomyopathy, skeletal and hematologic anomalies, and variable cognitive deficits (3–5). *PTPN11* encodes SHP2, a widely expressed cytoplasmic protein-tyrosine phosphatase that functions as a signal relay protein positively modulating RAS signaling (6). SHP2 is composed of two tandemly arranged N-terminal Src homology 2 (SH2) domains (N-SH2 and C-SH2), a catalytic domain (PTP), and a C-terminal tail with a role that is still not well characterized. The N-SH2 and C-SH2 domains control the subcellular localization and functional regulation of SHP2, with the former acting as an allosteric switch with two spatially nonoverlapping sites involved in an intramolecular inhibitory interaction with the PTP domain and in binding to phosphotyrosyl- (pY-) containing signaling partners (7). Crystallographic data indicate that the catalytically inactive conformation of SHP2 is

* This work was supported by grants from Telethon-Italy (GGP10020), ERA-Net for research programs on rare diseases 2009 (NSEuroNet), Programma di collaborazione Italia-USA 2010 (11US/10), and Associazione Italiana per la Ricerca sul Cancro (AIRC) (IG 13360) (to M. T.) and by grants from Telethon-Italy (GGP09243) and European Network of Excellence Experimental Network for Functional Integration (ENFIN) (to G. C.).
◆ This article was selected as a Paper of the Week.
⌘ *Author's Choice*—Final version full access.
[1] Both authors contributed equally to this work.
[2] To whom correspondence should be addressed: Dipartimento di Ematologia, Oncologia e Medicina Molecolare, Istituto Superiore di Sanità, Viale Regina Elena 299, 00161 Rome, Italy. Tel.: 39-06-49902569; Fax: 39-06-49902850; E-mail: mtartaglia@iss.it.

[3] The abbreviations used are: NS, Noonan syndrome; SH2, Src homology 2; PTP, protein-tyrosine phosphatase; PTPNS1, protein-tyrosine phosphatase nonreceptor type substrate 1; pY, phosphotyrosyl; BTAM, bisphosphotyrosyl-containing activation motif; MD, molecular dynamics.

stabilized by an extensive intramolecular binding network involving exposed residues of the N-SH2 and PTP domains. Upon engagement of the N-SH2 phosphopeptide-binding pocket, a conformational change of the domain weakens the autoinhibiting interdomain interaction, activating the phosphatase.

Previous work by our group and others provided evidence that NS-causing *PTPN11* mutations perturb the function of SHP2 through distinct molecular mechanisms (8–11). In most cases, lesions affect residues involved in the N-SH2/PTP interdomain binding network that stabilizes SHP2 in its autoinhibited state and up-regulate the function of SHP2 by perturbing the switching between the active and inactive conformations, favoring a shift in the equilibrium toward the former. There are, however, mutations affecting residues located far from the N-SH2/PTP-interacting surface. Among them, a few involve residues placed in the phosphopeptide-binding cleft of each SH2 domain and promote a gain of function of the enzyme by increasing binding affinity for pY-containing signaling partners or alter their binding specificity to those proteins. Of note, there are mutations that affect residues located within the PTP domain contributing to the stability of the catalytically inactive conformation but also participating in catalysis or controlling substrate specificity. For some of these NS-causing defects, biochemical data indicate that those substitutions favor protein activation by promoting dissociation of the N-SH2 and PTP domains without any substantial perturbing effect on catalysis. Other changes affecting the catalytic domain, as those underlying LEOPARD syndrome, a disorder that is clinically related to NS (12), however, have dramatic consequences on the catalytic function of SHP2 (9, 13, 14).

Available mutation data strongly support the idea that the specificity in the amino acid substitution is relevant to the functional dysregulation and disease pathogenesis of SHP2. A distinct class of activating mutations in *PTPN11* occurs largely as a somatically acquired event with variable prevalence in childhood hematological malignancies (9, 15–17). NS- and leukemia-associated mutations exert a differential perturbing effect on the function of SHP2, development, and hematopoiesis (9, 10, 18, 19). Similarly, among the mutations causing NS and LEOPARD syndrome, largely invariant amino acid changes are observed for several recurrently affected codons, indicating a specific role for the residue being introduced (9). Such an invariant occurrence of mutations can be ascribed to diverse driving forces due to either selection-by-function or site-specific increased mutability (11).

Here, by determining the biochemical behavior of all possible substitutions arising from single-base changes affecting codons 62 and 63, we explored the molecular mechanisms lying behind the largely invariant occurrence of the NS-causing Y62D and Y63C amino acid changes. We show that the autoinhibitory interaction between the N-SH2 and PTP domains is perturbed in both mutants as a result of an unanticipated extensive structural rearrangement of the N-SH2 domain rather than a consequence of a local effect. Our data also indicate that replacement of Tyr^{63} has an unexpected disruptive effect on the structure of the N-SH2 phosphopeptide-binding pocket implicated in the interaction of SHP2 with signaling partners and that the disease-causing mutation is the only substitution among all possible amino acid changes at that codon that perturbs the stability of the inactive conformation of SHP2 without severely impairing proper binding of N-SH2 to the phosphopeptide. On the other hand, the Y62D change is the only substitution at that codon destabilizing the autoinhibited conformation of SHP2, although such disruptive effect is balanced, in part, by less efficient binding properties of the mutant. Overall, our findings document that the selection-by-function mechanism acting as driving force for mutations affecting codon 62 and 63 implies the existence of counteracting effects operating on the allosteric control of the function of SHP2.

EXPERIMENTAL PROCEDURES

Expression Constructs—The full-length human polyHis-tagged *PTPN11* cDNA was cloned in a pET-26b vector (Novagen) using the HindIII and XhoI restriction sites. The 12 single-base changes resulting in amino acid substitutions at codons 62 and 63 (see Table 1) and the c.184_186delTACinsGAG change resulting in the tyrosine-to-glutamic acid amino acid substitution at codon 62 were introduced by site-directed mutagenesis (QuikChange site-directed mutagenesis kit, Stratagene). The polyHis- and GST-tagged N-SH2 domain constructs (residues 6–103) were PCR-generated and cloned in the pET-26b (Novagen) and pGEX-2TK (Amersham Biosciences) vectors. For cellular studies, the full-length *PTPN11* cDNA carrying the NS-causing c.184T>G (Y62D) and c.188A>G (Y63C) missense mutations were cloned in pcDNA6/V5-HisA (Invitrogen). The coding sequence of all constructs was confirmed by bidirectional sequencing. FLAG-Gab1 and HA-Erk2 constructs have previously been described (20).

ERK Phosphorylation Assay—293T cells were cultured in Dulbecco's modified Eagle's medium (VWR International PBI Srl) supplemented with 10% heat-inactivated fetal bovine serum (EuroClone) and 1% penicillin-streptomycin, at 37 °C with 5% CO_2. Constructs were cotransfected with HA-Erk2 and FLAG-Gab1 using *Trans*IT-LT1 transfection reagent (Mirus Bio LLC). ERK phosphorylation status was evaluated in time course experiments, basally and following EGF (Invitrogen) stimulation (30 ng/ml), as described previously (20). Following overnight incubation with anti-HA antibody (Sigma), immunoprecipitates were collected with protein G-Sepharose (Amersham Biosciences) for 2 h, washed, and analyzed by Western blotting using the anti-phospho-p44/42 MAPK (Thr^{202}/Tyr^{204}) antibody (Cell Signaling). Membranes were then stripped and probed with anti-HA antibody for protein normalization. To evaluate the SHP2-V5, FLAG-Gab1, and Erk2-HA protein levels, 30 μg of total lysates were immunoblotted with anti-V5 (Invitrogen), anti-FLAG (Sigma), and anti-HA monoclonal (Sigma) antibodies.

Protein Purification—Recombinant proteins were expressed as reported previously (11), using *Escherichia coli* (DE3) Rosetta2-competent cells (Novagen). Following isopropyl-1-thio-β-D-galactopyranoside induction at 30 °C, harvesting, and cell lysis, polyHis-tagged full-length SHP2 proteins and the isolated N-SH2 domains were purified by chromatography, using the nickel-nitrilotriacetic acid magnetic agarose beads (Qiagen), and stored at −20 °C with 5 mM DTT. GST-tagged N-SH2

domains were purified using the glutathione-Sepharose beads (Amersham Biosciences) and stored at −80 °C with 20% glycerol.

Phosphatase Assays—Catalytic activity of wild-type SHP2 and generated mutants was evaluated *in vitro* using 20 pmol of purified recombinant proteins in a 200-μl reaction buffer (25 mM HEPES, pH 7.2; 50 mM NaCl; 2.5 mM EDTA; 62.5 mg/ml BSA; 5 mM DTT) supplemented with 20 mM *p*-nitrophenyl phosphate (Sigma) as substrate, either in basal condition or in the presence of the protein-tyrosine phosphatase nonreceptor type substrate 1 (PTPNS1) bisphosphotyrosyl-containing activation motif (BTAM peptide, hereinafter) (GGGGDIT-(pY)ADLNLPKGKKPAPQAAEPNNHTE(pY)ASIQTS) (Primm), and incubated at 30 °C for 30 min. Reactions were stopped with 0.1 N NaOH. Phosphate release was determined by measuring A_{405}. Amount, purity, and integrity of recombinant proteins were assessed using the protein assay kit (Bio-Rad) and Coomassie Blue staining.

Structural Interpretation and Molecular Dynamics Simulations—Electrostatic calculations were performed with the APBS 1.3 program (21), using the protein coordinates of the Protein Data Bank (PDB) entry 2shp (7), and calculating the electrostatic potential generated by the PTP domain (residues 221–524) on the surface of the N-SH2 domain. The linearized Poisson-Boltzmann equation was solved by the automatically configured sequential focusing multigrid algorithm, considering a dielectric constant of 2 and 78.54 for the solute and the solvent, respectively, with single Debye-Hückel boundary conditions, a probe radius of 1.4 Å, and a temperature of 300 K.

Molecular dynamics (MD) simulations were performed using GROMACS 4.0.4 (22), with the GROMOS96 ffG43a1 force field (23). Starting coordinates of the N-SH2 domain of human SHP2 were taken from PDB entry 2shp (chain A; residues 2–104) (7). The program DeepView 4.0.1 (24) was used to insert mutations at position 62 or 63. Rotamers with the lowest energy score were selected. The N and C termini of the protein were assumed to be charged. Protein was centered in a triclinic box and hydrated with more than 5,000 water molecules. The system equilibration was performed by a two-step energy minimization, first restraining all protein atoms to their positions and then removing the restraints. Following initial energy minimizations and a 100-ps MD run during which the protein atoms were position-restrained, the temperature of solute and solvent was raised to 300 K in a stepwise manner, performing four MD runs, 50 ps each, at different temperatures (50, 100, 200, and 250 K). Electrostatic interactions were calculated using the particle mesh Ewald method and a 1.2-nm cut-off radius for the real part calculation. van der Waals interactions were calculated using a cut-off radius (1.2 nm). The simple point charge model was used for water (25), and water geometry was constrained with the SETTLE algorithm (26). A Berendsen thermostat, with a coupling constant of 0.1 ps, was applied in all simulations (27), and the reference temperature was set to 300 K, except where stated otherwise. Pressure coupling was applied employing the Berendsen scheme, with a time constant of 1.0 ps, a reference pressure of 1 bar, and a compressibility of $4.5\ 10^{-5}\ \mathrm{bar}^{-1}$. Bond lengths were constrained with the LINCS algorithm (28). Simulations were run with a 2-fs time step and were at least 100 ns long. Translational and rotational motions of the protein were removed by least square fitting the positions of the C_α carbon atoms of the most rigid residues in the protein (residues 6–8, 27–32, 42–46, 52–57, 75–80, and 97–102) to their starting coordinates.

To evaluate the conformational variations of loop DE (residues 60–63), the distance between the center of mass of the DE loop backbone and the center of mass of the backbone of residues 75–77 of helix B was calculated. Root mean square positional fluctuations of C_α atoms were calculated according to standard definitions, between 15 and 100 ns. Molecular graphics were obtained with MOLMOL (29) and the Chimera visualization system (30).

Chemical Denaturation Assays—Intrinsic fluorescence spectra were measured on a Fluoromax 2 fluorometer (Horiba), with excitation at 295 nm and 3-nm band pass. Emission spectra were collected between 305 and 400 nm, and background was subtracted. The protein was dissolved in a 5 mM HEPES buffer, 75 mM NaCl (pH 7.2), at a 5 μM concentration, in a 3 × 3-mm path length cell. Temperature was controlled with a thermal bath to 20.0 ± 0.1 °C. After the addition of the chaotropic agent guanidinium chloride (Fluka), equilibration of the system was ensured by acquiring multiple spectra until no further changes were observed.

Surface Plasmon Resonance Analysis—Surface plasmon resonance measurements were performed using a BIAcoreX instrument (BIAcore International AB) equipped with two flow-cell sensor chips. Biotinylated BTAM peptide (100 μg/ml) or the monophosphorylated N-terminal portion of that peptide (GGGGDIT(pY)ADLNLPKGKK) was resuspended in a buffer containing 10 mM HEPES (pH 7.4), 150 mM NaCl, 3 mM EDTA, and 0.005% (v/v) surfactant P20 and injected over a streptavidin-coated sensor chip, at a flow rate of 10 ml/min for 2 min, to obtain an immobilization level of 800 resonance units. The biotin molecule was linked to the N terminus of the peptide by a stretch of polyglycine. Wild-type and mutant polyHis-tagged N-SH2 domains were resuspended in the same buffer and applied at a concentration of 500 nM, with a flow rate of 30 ml/min. The amount of protein bound to the sensor chip was monitored by the change in refractive index, given in arbitrary response units, at 25 °C, as a function of time. At the end of the sample plug, the buffer was passed over a sensor surface to allow dissociation. The sensor surface was regenerated for the next sample using a 2-μl pulse of 35 mM NaOH. As a control, no binding was observed when polypeptides were run on the flow-cell sensor chip with immobilized biotin.

Phosphopeptide Array Binding Analyses—Chip arrays used to characterize the N-SH2 recognition specificity consisted of 6,057 13-mers, each displaying a phosphorylated tyrosine residue at position 7 (31). One-fourth of these phosphopeptides were retrieved from Phospho.ELM (32), whereas the remaining received a high score according to the NetPhos Neural Network predictive algorithm (33). The list of phosphopeptides is available upon request. The library was arranged together with control spots on a glass slide in three identical subarrays of 6,400 dots. Control spots included PBS and FLAG epitope peptides (negative controls), IgG or IgM antibodies (controls for secondary antibody binding), and GST protein (positive control for the

primary antibody). Tetramethyl-5-carboxyrhodamine and Cy3 dyes were spotted to facilitate grid orientation. Sixty peptides were spotted in triplicate to verify within-array reproducibility. Following a 1-h blocking in 5% BSA-containing PBS, the phosphopeptide arrays were probed with 1 μg/ml of each GST-tagged N-SH2 domain. After washing, chips were incubated with an anti-GST Cy-5-conjugated antibody (Amersham Biosciences), and fluorescence signals were revealed with a ScanArray Gx Plus instrument (PerkinElmer Life Sciences). To determine a positive data set of interacting peptides, the fluorescence intensity of each spot was measured, and the median intensity of the three replicated spots was computed for each of the 6,400 phosphopeptides, which were ordered according to their median fluorescence intensity. Peptides whose binding intensities differed from the average intensity by more than 3 standard deviations (z score >3) were considered as "binders." For each N-SH2 domain, the enrichment in specific residues at the different positions flanking the pY was visualized by using Two Sample Logo representations (34).

SPOT synthesis technology was used to synthesize a subset of opportunely selected phosphopeptides on the cellulose membrane, as described previously (35). Membranes were incubated with the N-SH2^{wt}, N-SH2^{Asp62}, and N-SH2^{Asp63} domains expressed as GST-tagged fusion proteins. Binding efficiency and affinity were revealed using an anti-GST antibody conjugated to horseradish peroxidase fluorophore. Signal intensity was quantified, and the -fold increase (normalized to the signal obtained for the wild-type N-SH2 domain) was plotted. As positive controls, peptides containing the phosphorylated binding motif of GAB1 and PTPNS1 specifically recognized by the N-SH2 domain of SHP2 were also spotted. Binomial testing and $p < 0.05$ were applied.

RESULTS

Activity of SHP2 Mutants—Available published records document that *PTPN11* mutations affecting codons 62 and 63 are a relatively common event among individuals with NS, accounting for ~10% of *PTPN11* mutation-positive cases (Table 1). These missense substitutions have not been observed to occur as somatic changes in cancer. At the nucleotide level, a largely invariant occurrence for the c.184T→G transversion (Y62D) is observed, whereas the A → G transition at nucleotide 188 (Y63C) is the only change occurring at this codon reported so far. None of those codons encompasses a CpG dinucleotide. Assuming similar mutation rates for all the possible single-nucleotide substitutions affecting each codon and functional equivalence of the resulting amino acid changes, the frequency of these missense mutations is significantly higher than that expected simply by chance (Y62D, $p = 2.1 \times 10^{-19}$; Y63C, $p = 7.3 \times 10^{-53}$), supporting the idea of a selection-by-function mechanism operating on this nonrandom distribution of amino acid changes affecting both codons.

Tyr^{62} and Tyr^{63} are located at the PTP-interacting surface of the N-SH2 domain, and lesions affecting these codons were predicted to perturb the equilibrium between the inactive and active conformation of the protein by affecting the stability of the autoinhibitory N-SH2/PTP interdomain interaction (Fig. 1) (8, 9). Consistent with the predicted activating role of both the NS-causing Y62D and the NS-causing Y63C amino acid substitutions, ectopic expression of the V5-tagged SHP2^{Asp62} and SHP2^{Cys63} mutants in 293T cells promoted enhanced ERK phosphorylation upon EGF stimulation when compared with that observed in cells expressing the wild-type protein (Fig. 2). To explore the consequences of the Y62D and Y63C amino acid changes on the biochemical behavior of SHP2 and provide an explanation for their largely invariant occurrence in NS, all possible mutants arising from single-base changes affecting those codons, as well as the wild-type protein, were expressed in bacteria and purified, and their phosphatase activities were determined *in vitro*, basally and following stimulation with the BTAM peptide previously demonstrated to activate SHP2 (11, 36). Under basal conditions, all but one SHP2 mutant at codon 62 exhibited a relatively low catalytic activity, which was comparable with that observed for the wild-type protein (V_{max} = 6.8 pmol/min/pmol), the exception being the NS-causing SHP2^{Asp62} that showed a 2.3-fold increase in substrate dephosphorylation (Fig. 3*A*). The activating effect of the Y62D substitution was weaker when compared with that promoted by the leukemia-associated E76K change, but consistent with what has previously been described for most NS-causing lesions affecting residues located at the N-SH2/PTP interface (9, 10). Following BTAM stimulation, mutants not associated with NS showed either an increase in phosphatase activity comparable with that observed for the wild-type protein (SHP2^{His62}, SHP2^{Cys62}, and SHP2^{Phe62}) or a slightly enhanced catalytic activity (SHP2^{Asn62} and SHP2^{Ser62}) that was, however, significantly lower than that characterizing the NS-causing mutant ($P_{Student's\ t\ test} < 0.005$, in all comparisons). Based on the nature of the amino acid change, a trivial interpretation of the perturbing effect of the Y62D substitution on the stability of the N-SH2/PTP interaction would imply a possible electrostatic

TABLE 1

List of the disease-causing amino acid substitutions arising from single-base changes at codons 62 and 63 of the *PTPN11* gene

Data are from the database reported by Tartaglia *et al.* (9) updated to April 2011. The complete list of somatically acquired and germline-transmitted disease-causing *PTPN11* mutations and relevant references are available upon request.

Affected residue	Nucleotide substitution	Introduced residue	Occurrence (n = 855)	Associated phenotype
Tyr^{62}	c.184T→A	Asn	1	NS
	c.184T→C	His		
	c.184T→G	Asp	24	NS
	c.185A→C	Ser		
	c.185A→G	Cys	1	—[a]
	c.185A→T	Phe		
	c.186C→A	*Stop codon*		
	c.186C→G	*Stop codon*		
	c.186C→T	*Silent change*		
Tyr^{63}	c.187T→A	Asn		
	c.187T→C	His		
	c.187T→G	Asp		
	c.188A→C	Ser		
	c.188A→G	Cys	67	NS
	c.188A→T	Phe		
	c.189T→A	*Stop codon*		
	c.189T→C	*Silent change*		
	c.189T→G	*Stop codon*		

[a] This amino acid change was documented to be germline-transmitted in a subject with neuroblastoma without clinical features supporting a diagnosis of NS, suggesting that it might represent a private variant causally unrelated to disease. Parental DNAs were not available to verify the *de novo* occurrence of this variant.

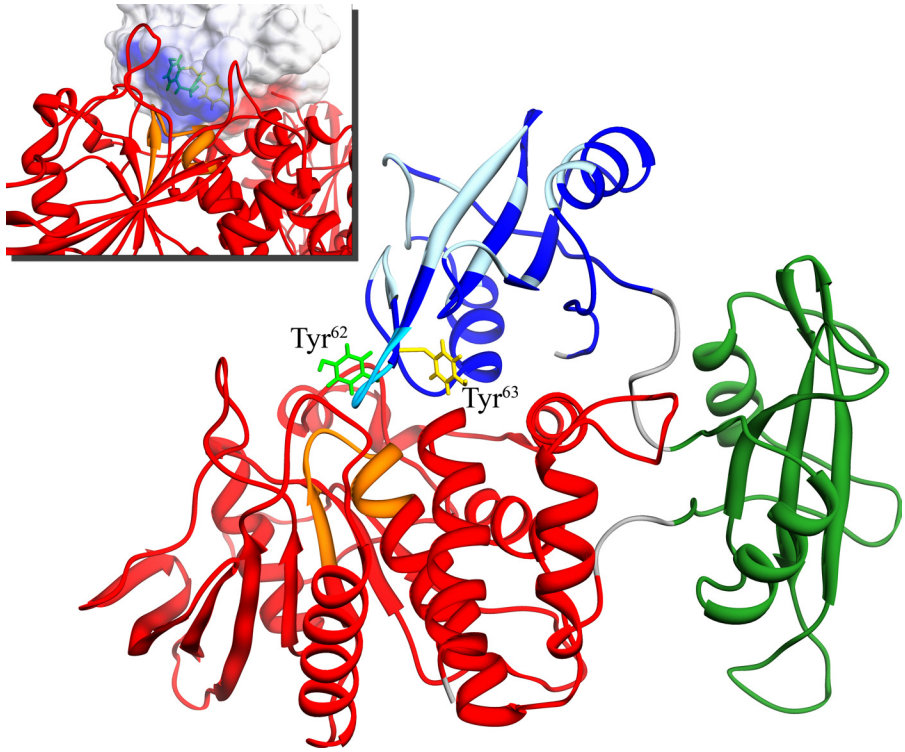

FIGURE 1. **Structure of SHP2 in its catalytically inactive conformation and location of Tyr^{62} and Tyr^{63}.** The N-SH2, C-SH2, and PTP domains of the protein (residues 2–525; PDB entry 2shp, chain A) are shown in *blue*, *green*, and *red*, respectively. The signature motif of the PTP active site (*orange*), N-SH2 blocking loop (*cyan*), and N-SH2 phosphopeptide-binding cleft (according to the x-ray structure of the N-SH2-peptide complex, PDB entry 1aya) (*light blue*) are also displayed. The side chains of residues Tyr^{62} and Tyr^{63} are reported in *green* and *yellow*, respectively. Residues missing in the experimental crystallographic structure were reconstructed as described previously (21). The *inset* shows the electrostatic potential generated by the PTP domain on the N-SH2 surface in the catalytically inactive conformation of SHP2. The PTP backbone is reported as a *ribbon*, and the N-SH2 surface is shown. *Red* and *blue colors* indicate negative and positive potential values ranging from −40 *kT*/*e* to +40 *kT*/*e*, respectively. The side chains of residues Tyr^{62} and Tyr^{63} are shown as above.

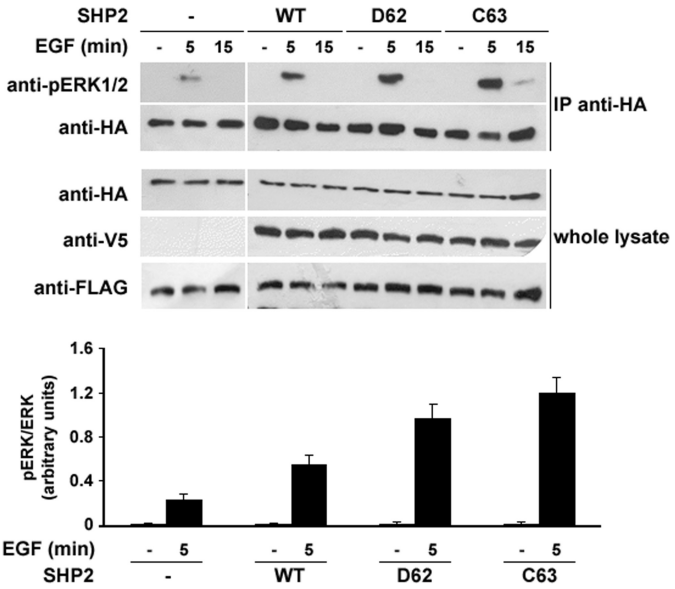

FIGURE 2. **ERK phosphorylation assays.** 293T cells were co-transfected with HA-tagged ERK2, FLAG-Gab1, and the indicated V5-tagged SHP2 constructs. Following starvation (12 h) and EGF stimulation (30 ng/ml), cells were immunoprecipitated (*IP*) with anti-HA antibody and probed with phosphorylated ERK1/2 (*anti-pERK1/2*) or anti-HA antibodies. Aliquots of corresponding cell lysates were probed with anti-V5, anti-HA, and anti-FLAG antibodies. Representative blots (above) and mean ± S.D. densitometry values (below) of three independent experiments are shown.

repulsive mechanism resulting from the introduction of a charged side chain at the interface of the two domains. Assessment of the *in vitro* phosphatase activity of the SHP2^{Glu62} mutant (c.184_186delTACinsGAG), however, indicated only a moderate activation when compared with the disease-causing SHP2^{Asp62} protein, both basally and following BTAM stimulation, suggesting a more complex role for the tyrosine-to-aspartic acid change in perturbing the function of SHP2.

Biochemical analysis performed on the panel of generated mutants at codon 63 provided evidence that, with the exception of SHP2^{His63} and SHP2^{Phe63}, which showed activities comparable with the wild-type protein, mutants exhibited a variable increase in their activation basally (Fig. 3*A*), indicating that most mutations at this codon perturbed the stability of the enzyme in its catalytically inactive conformation. Of note, basal phosphatase activity of the NS-causing SHP2^{Cys63} mutant was only 1.6-fold higher than that of the wild-type protein and considerably lower than that characterizing the SHP2^{Asp63} mutant, indicating only a mild destabilizing effect of this substitution on the N-SH2/PTP interdomain interaction. Following BTAM stimulation, however, most mutants at this codon appeared unresponsive (SHP2^{Asp63}) or poorly responsive (SHP2^{Asn63}, SHP2^{His63}, and SHP2^{Ser63}), suggestive of an unpredicted disruptive effect of these amino acid changes on the N-SH2 pocket involved in phosphopeptide binding. In contrast, the NS-causing SHP2^{Cys63} mutant exhibited markedly augmented catalytic activation ($P_{\text{Student's } t \text{ test}} < 0.05$, in comparison with SHP2^{Phe63}

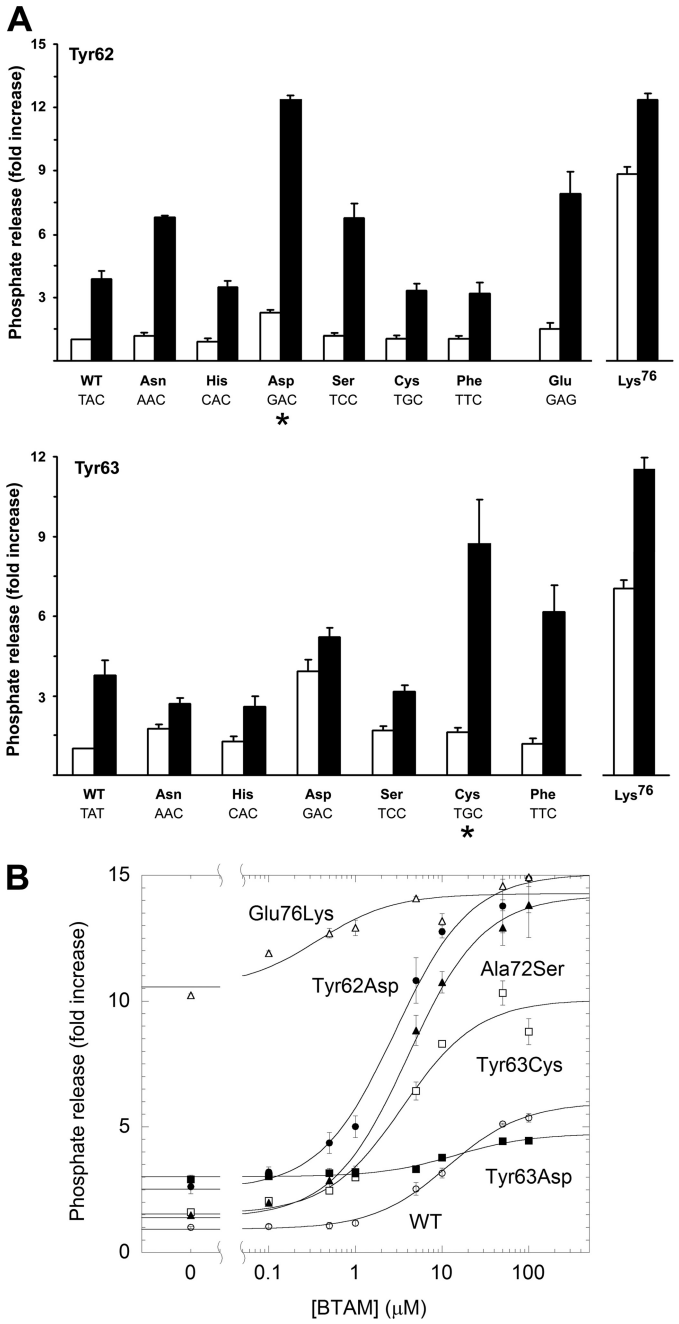

FIGURE 3. **Biochemical characterization of SHP2 mutants.** *A*, *in vitro* phosphatase assay of wild-type SHP2 and all mutants arising from a single-base change at codons 62 and 63. Mutants carrying the Y62E substitution and the leukemia-associated E76K change are also shown for comparison. Catalytic activity was measured as pmoles of phosphate released using *p*-nitrophenyl phosphate as a substrate, basally (*white bars*) and following stimulation with 10 μM BTAM peptide (*black bars*). Values are expressed as mean ± S.D. of at least three independent experiments and are normalized to the basal activity of the wild-type SHP2. *Asterisks* indicate the recurrent NS-causing amino acid substitutions. *B*, *in vitro* phosphatase assay of wild-type SHP2 and mutant proteins as a function of BTAM peptide concentration. Catalytic activity (mean values ± S.D. of three independent experiments) was measured as above.

and SHP2^{Asp63}; $P_{\text{Student's } t \text{ test}} < 0.002$, in all other comparisons).

The catalytic activity of the NS-causing SHP2^{Asp62} and SHP2^{Cys63} mutants was then measured as a function of BTAM concentration and compared with a panel of selected proteins (Fig. 3*B*). Both the pathogenetic mutants were significantly more responsive to peptide stimulation than the wild-type protein. Such enhanced responsiveness is predicted to be a direct consequence of the perturbing effect of these lesions on the N-SH2/PTP interaction network because the "open" conformation implies an enhanced binding affinity for the phosphopeptide (37). Although the increased basal activity of these mutants indicates a destabilization of the inactive conformation of the phosphatase, supporting the idea that a shift in the conformational equilibrium is definitely contributing to their higher responsiveness, the possibility that those lesions might perturb the binding properties of the N-SH2 domain due to a concomitant structural rearrangement of the phosphopeptide-binding cleft could not be ruled out. Consistent with this hypothesis and the above observations, the basally hyperactive SHP2^{Asp63} protein was essentially unresponsive at all the investigated BTAM concentrations, indicating impaired phosphopeptide binding. Overall, our data were consistent with a selection-by-function model implicating the destabilization of the N-SH2/PTP interdomain interaction as primary driving force, but highlighted an unexpected counteracting perturbing effect of a subset of mutations affecting residues 62 and 63 on the proper binding of SHP2 to its signaling partners.

Consequences on N-SH2 Domain Structure—Both the NS-causing SHP2^{Asp62} and SHP2^{Cys63} mutants were found to be basally activated and exhibited enhanced responsiveness to BTAM stimulation. Structural analyses were performed to understand the molecular mechanism(s) underlying such a hyperactive behavior. As anticipated, the Y62D substitution introduces a charged side chain at the interface between the N-SH2 and PTP domains, which might be suggestive of structural stress due to the introduction of electrostatic repulsion between the surfaces of these domains, analogous to what had previously been recognized for the leukemia-associated E76K amino acid change (37). Poisson-Boltzmann calculations of the electrostatic potential generated by the PTP domain on the N-SH2 surface, however, indicated that the side chain of the aspartic acid is introduced in a region of positive potential generated by several cationic residues, including Lys^{364} and Lys^{366} (Fig. 1). Based on these considerations, the Y62D substitution would be expected to generate electrostatic attraction between the two domains, predicting a more steady interdomain interaction, in contrast to the observed biochemical behavior. This apparently conflicting evidence suggested that the Y62D substitution might lead to a more complex structural rearrangement of the N-SH2 domain, rather than to a mere perturbation of the N-SH2/PTP interaction. This hypothesis was also consistent with the observed impaired or less efficient responsiveness of the majority of mutants at codon 63 to the BTAM peptide, notwithstanding their basal activation, implying a structural adjustment of the phosphopeptide-binding pocket of the N-SH2 domain.

To characterize such perturbing effect(s), MD simulations of the isolated N-SH2 domain carrying either the NS-causing amino acid changes or the Y63D substitution, the latter included as a representative of unresponsive mutants, were carried out. Simulations started from the structure of the N-SH2 domain in the crystal structure of the whole protein in its auto-

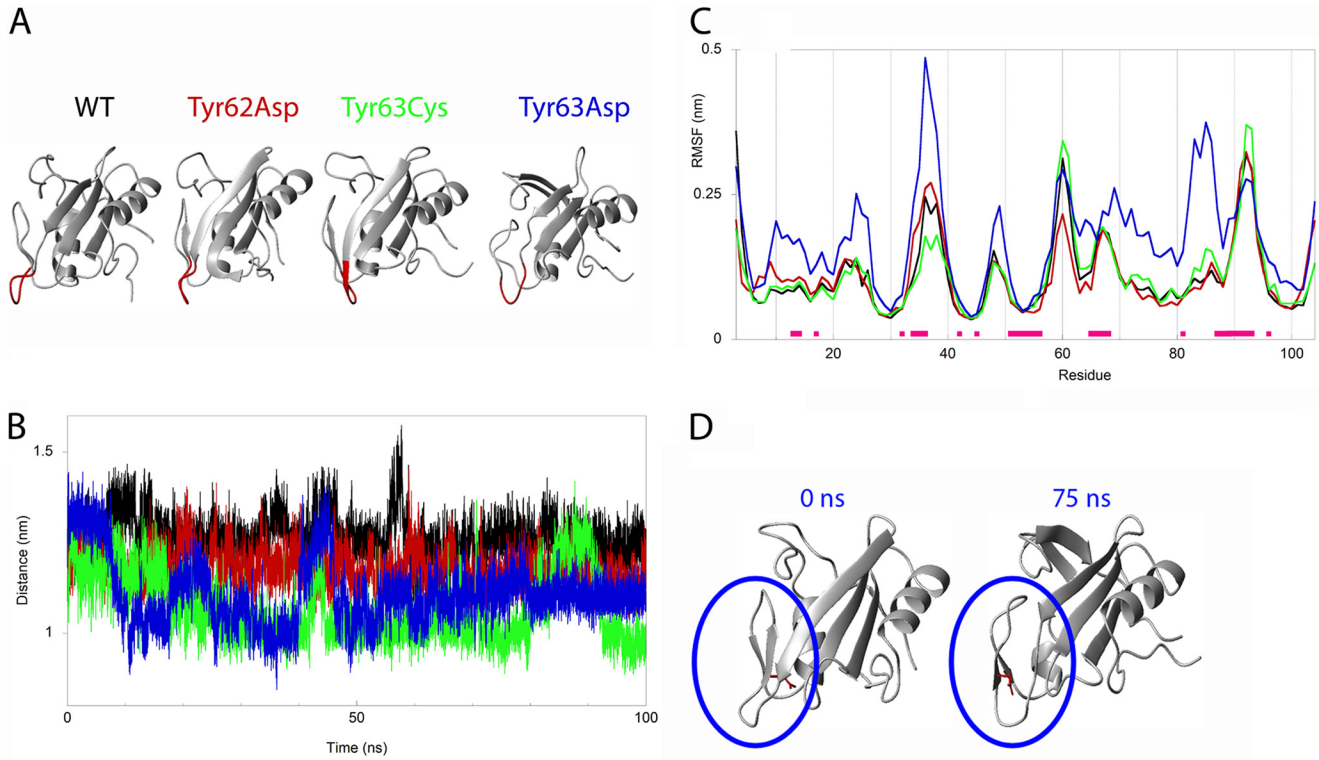

FIGURE 4. **Molecular dynamics simulations.** *A*, ribbon representation of the final structures obtained from simulations of the N-SH2 domain for wild-type (*WT*), Y62D, Y63C, and Y63D mutants. The blocking loop (residues 58–62) is shown in *red*. *B*, time evolution of the distance between the blocking loop and the B-helix located behind it during simulations. *C*, root mean square positional fluctuations (*RMSF*) of the C_α atoms of the wild-type (*black*), Y62D (*red*), Y63C (*green*), and Y63D (*blue*) N-SH2 domains during simulations. *Magenta marks* indicate residues belonging to the phosphopeptide-binding pocket, as defined previously (21). *D*, ribbon representation of two frames extracted from the Y63D N-SH2 simulation. Asp^{63} is shown as *red sticks*. The *blue circles* indicate the region undergoing the main conformational transitions.

inhibited conformation, in which the blocking loop of the N-SH2 domain (residues 58–62) obstructs the catalytic site of the PTP domain. Notably, the conformation of this loop during the MD trajectories changed significantly in all mutants, undergoing a conformational transition that led it to fold back onto the domain surface (Fig. 4*A*), reducing its spatial distance with the B helix located behind it (Fig. 4*B*). Among the mutants, the structure of N-$SH2^{Asp63}$ was found to be less stable when compared with those of the others, as indicated by the higher root mean square fluctuations of its C_α atoms (Fig. 4*C*). These findings indicated that all mutations induced a significant conformational rearrangement of the N-SH2 domain, predicted to reduce the ability of its blocking loop to inhibit the catalytic site of the enzyme, which would favor a shift of the equilibrium toward the active shape of the protein. Such an effect, most probably, underlies the increased basal activity of each mutant.

MD simulations also indicated that the structural origin of the perturbing effect promoted by each mutation differed significantly. In the wild-type protein, the tyrosine residue at position 63 participates to the hydrophobic core of the N-SH2 domain that also involves residues Phe^{41}, Ile^{56}, Leu^{65}, Phe^{71}, Ala^{72}, Leu^{74}, and Leu^{77}. Although the Y63C substitution was predicted to disrupt this region, creating a cavity in it, the effect of the Y63D change could be even more radical because of the insertion of a charged residue in the hydrophobic pocket. Consistent with this observation, during the trajectory of the N-$SH2^{Asp63}$ mutant, the side chain of the aspartic acid moved toward the protein surface to maximize its solvent exposure, leading to a significant distortion of the entire domain structure (Fig. 4*D*). In contrast, the Y62D mutation introduced a charged side chain in the water-exposed surface of the protein, which would be expected to cause a perturbation in the network of electrostatic interactions within the blocking loop region. In particular, although a stable salt bridge between residues Asp^{64} and Lys^{70} occurred in the wild-type protein, the side chain of Lys^{70} reoriented to interact with both the aspartic acid residues at positions 62 and 64 in the mutant. In addition, the Y62D amino acid change was predicted to introduce a direct repulsion between Asp^{61} and Asp^{62}, which are located in the blocking loop, contributing to the perturbation of the local structure and dynamics of this region.

To confirm the structural data experimentally, chemical denaturation curves were obtained by measuring the intrinsic fluorescence of each protein, as a function of guanidinium chloride concentration (Fig. 5). The emission spectra of all mutants were shifted to longer wavelengths when compared with that characterizing the wild-type N-SH2 domain, even under non-denaturing conditions, indicating a higher solvent exposure of the single tryptophan residue of the domain. Because this amino acid is located at position 6, which is spatially far from the site of mutations, this effect indicated a constitutive change in the overall conformation of the N-SH2 domain. In all mutants, the unfolding transition took place at lower guanidinium chloride concentrations when compared with the wild-type protein, providing further support for a structural disrupting effect of these amino acid changes. As expected, the effect

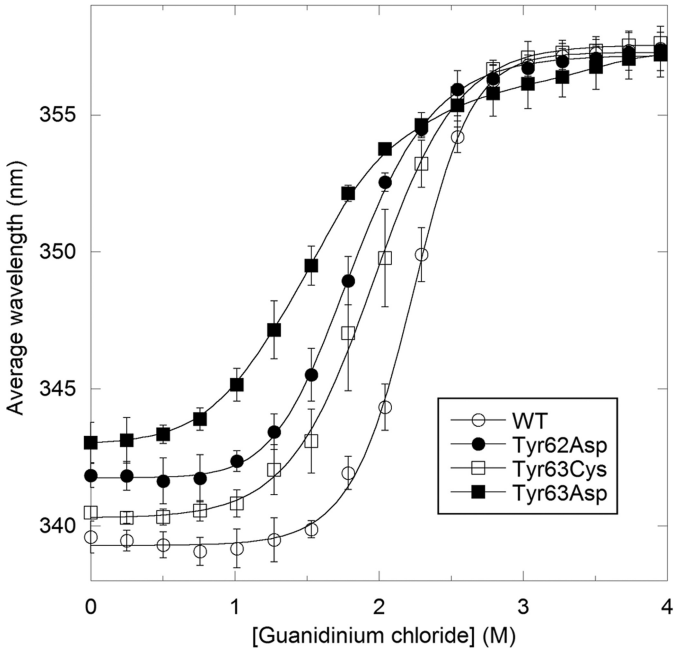

FIGURE 5. **Chemical denaturation of the isolated wild-type and mutant N-SH2 domains, as indicated by the shift in the fluorescence spectrum of Trp[6].** Protein unfolding leads to exposure of the fluorophore to the water environment, resulting in a red shift in the spectrum. Average wavelength was calculated according to the following equation: $\Sigma^i\lambda^iF^i/\Sigma^iF^i$, where F represents fluorescence intensity and λ represents the wavelength at which it was measured. Values are expressed as mean ± S.D. of three independent experiments.

was significantly larger for the N-SH2^{Asp63} mutant, confirming the dramatic structural perturbation predicted by MD simulations on the whole N-SH2 domain, including its phosphopeptide-binding site.

BTAM Binding Properties—Biochemical and structural data indicated that most mutants at codon 63 were unresponsive or only slightly responsive to the BTAM peptide, suggesting that these lesions could affect peptide binding affinity. To explore further the unpredicted effect of mutations at codons 62 and 63 on N-SH2 domain function, the binding properties of the isolated N-SH2 domains carrying the NS-causing Y62D and Y63C changes were compared with those of N-SH2 domains from the apparently unresponsive SHP2^{Asp63} and wild-type proteins using surface plasmon resonance analysis. Following injection of biotinylated BTAM peptide over a streptavidin-coated sensor chip, recombinant proteins were applied at a concentration of 500 nM, and the amount of bound protein was monitored by the change in refractive index as a function of time. Surface plasmon resonance analysis indicated that the N-SH2^{Cys63} mutant had a binding affinity comparable with that observed for the wild-type domain (Fig. 6*A*). On the other hand, consistent with structural and biochemical data, the N-SH2^{Asp63} mutant was almost completely unable to bind the phosphopeptide, providing direct evidence for the disruptive effect exerted by a mutation affecting a residue located in the N-SH2/PTP-interacting surface on the phosphopeptide-binding cleft function. The N-SH2^{Asp62} domain exhibited an intermediate behavior, as it retained a significant affinity for the BTAM peptide, although significantly reduced when compared with the wild-type domain. These findings were confirmed using the N-ter-

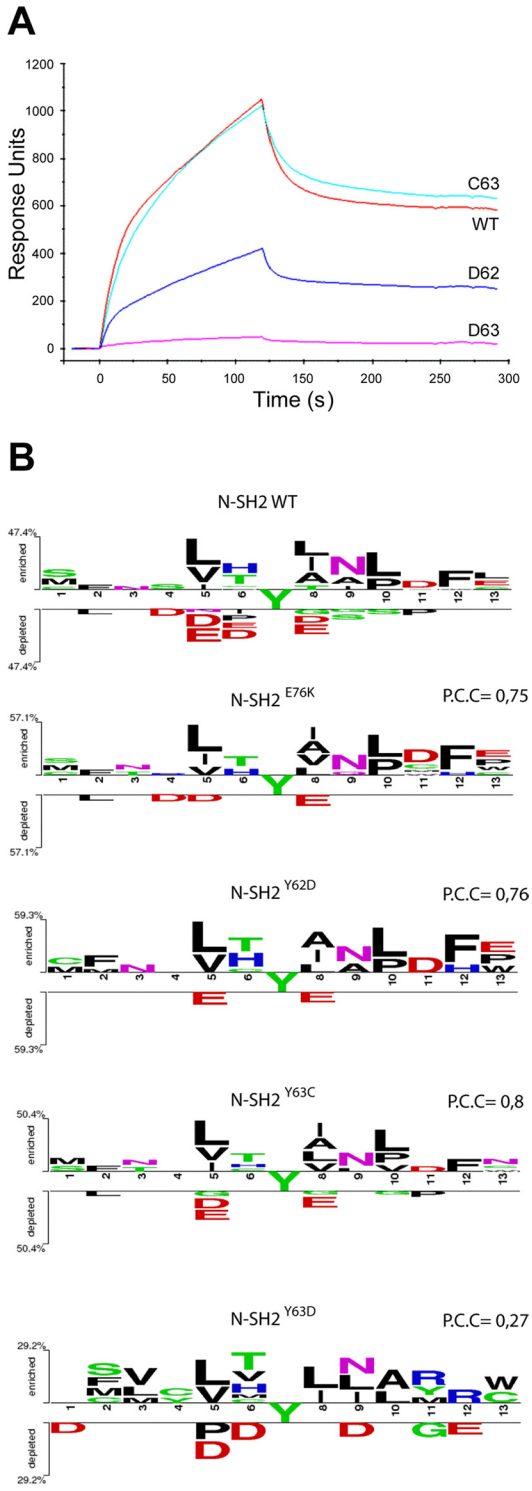

FIGURE 6. **Phosphopeptide binding properties of wild-type and mutant N-SH2 domains.** *A*, surface plasmon resonance analysis. Sensorgrams of the interaction of the wild-type protein (*red*) and the Y62D (*blue*), Y63C (*cyan*), and Y63D (*pink*) SHP2 mutants with the biotinylated BTAM peptide are shown. *B*, Two Sample Logo representation of the binding recognition specificity of wild-type and mutant N-SH2 domains. Each logo abridges the residue enrichment at the positions flanking the phosphorylated tyrosine in the best ligand peptides. At each position of the *top diagram*, the overall stack height indicates the sequence conservation, whereas the height of symbols within each stack indicates the relative frequency of the indicated residue. The *bottom diagram* illustrates the "anti-motif" (*i.e.* residues that are enriched at each position in the peptide sequences of the negative set) ($P_{Student's\ t\ test} < 0.05$). Residue positions are numbered by referring their position to that of the pY. The Pearson correlation coefficient (*P. C. C.*) between the wild-type N-SN2 domain and each mutant is also shown.

minal portion of the BTAM peptide phosphorylated at the tyrosine residue known to bind specifically the N-SH2 domain of the phosphatase (36) (data not shown).

Consequences on Phosphopeptide Recognition and Binding Specificity—Aside from their effect on binding affinity, the predicted structural rearrangements of the N-SH2 domain in mutants at codons 62 and 63 might also perturb the recognition specificity for pY-containing signaling partners. To explore this possibility, bacterially expressed wild-type and mutant forms of the N-SH2 domain were challenged against an array of 6,057 pY-containing naturally occurring peptides known or predicted to be phosphorylated *in vivo*. Array binding assays were also performed on the N-SH2 domain carrying the leukemia-associated E76K amino acid substitution, as representative of the activating mutations acting merely locally to disrupt the stability of the autoinhibitory N-SH2/PTP interdomain interaction (37). Consistent with available published data (11, 38–40), the residues of the phosphopeptide that appeared to mediate binding specificity to the wild-type domain were at −2, −1, +1, +2, and +3 from the phosphotyrosine, as shown by the generated sequence logo, which abridges the residue enrichment at each position flanking the phosphotyrosine in the best ligand peptides (Fig. 6*B*). Those positions were found to bear the highest information content also in N-SH2^{Lys76}, N-SH2^{Asp62}, and N-SH2^{Cys63} binding. For each mutant, a pairwise comparison of phosphopeptide binding profiles was determined by direct comparison of the median fluorescence intensity of each binder with those measured for the wild-type domain. This analysis documented that all the phosphopeptides identified as high affinity binders for the wild-type domain were also recognized as good ligands of the N-SH2^{Lys76} domain, with an overall correlation coefficient of 0.75. A similar behavior was observed for the N-SH2^{Asp62} and N-SH2^{Cys63} mutants (correlation coefficients equal to 0.76 and 0.80, respectively), providing evidence that both domains retained recognition specificity comparable with that observed for the wild-type counterpart. In contrast, the Y63D amino acid change was found to substantially perturb both affinity and specificity, as indicated by the relatively small number of shared binders with the wild-type domain (correlation coefficient = 0.27) and a general more promiscuous behavior.

To further investigate these observations, a selected panel of phosphopeptides, which were predicted to represent the high affinity binders of the wild-type and mutated N-SH2 domains by fitting their sequence consensus motifs, were synthesized by SPOT synthesis technology, and binding properties of the N-SH2^{Asp62} and N-SH2^{Asp63} domains were assayed (Fig. 7). In line with our previous findings, the N-SH2^{Asp62} mutant was found to bind a significantly smaller number of peptides when compared with the wild-type domain, suggesting an overall less efficient binding, whereas the N-SH2^{Asp63} domain displayed substantially different binding preferences from both the N-SH2^{Asp62} and the wild-type domain. For the latter, the analysis confirmed a defective binding to the N-SH2 domain-specific PTPNS1 phosphorylated motif as well as to the majority of phosphopeptides inferred to represent efficient binders of the wild-type N-SH2 domain.

DISCUSSION

In this study, we explored the molecular mechanisms involved in the functional dysregulation of SHP2 caused by missense changes at codons 62 and 63 and characterized the driving force underlying the largely invariant occurrence of the recurrent Y62D and Y63C amino acid substitutions causing NS. Structural and biochemical data demonstrated that the two disease-causative lesions are the only substitutions promoting a significant up-regulation of the function of SHP2 among all possible changes resulting from a single-base mutation affecting each codon. As observed for other mutations affecting exposed residues located at the interface of the N-SH2 and PTP domains, most mutations at these codons disrupted the autoinhibitory interaction between the two domains. Unexpectedly, the hyperactive behavior of both mutants was found to be the result of a substantial structural rearrangement of the N-SH2 domain that also involved the phosphotyrosine-binding pocket mediating the interaction of SHP2 with signaling partners and was demonstrated to affect the phosphopeptide-binding capability of the domain in a subset of mutants. These findings imply the existence of counteracting effects of these mutations operating on the control of the function of SHP2.

SHP2 is regulated by an allosteric switch involving the N-SH2 domain, in which two distinct sites participate in an intramolecular interaction with the PTP domain and in binding to a pY-containing signaling partner (7). These sites function with negative cooperativity and mediate the conformational transition controlling the inactive and active states of the phosphatase (7, 41, 42). In the absence of a pY-containing partner, SHP2 assumes an autoinhibited state, as evinced *in vitro* by the low phosphatase activity of the unstimulated enzyme, whereas the N-SH2 domain loses surface complementarity for its binding site on the PTP domain (7) and overall binding affinity with it (43) in its rearranged phosphopeptide-bound state. This model predicts that dysregulation of the function of SHP2 can result from structural perturbations involving each of the two interactions. Indeed, previous work by our group and others confirmed that different mechanisms are operating at both these N-SH2 sites for NS-causing *PTPN11* mutations (9–11). In most cases, mutations affect the N-SH2/PTP interdomain binding network locally, destabilizing the inactive conformation of the protein. A subset of mutations, however, can act by increasing the binding affinity of SHP2 for pY-containing partners or altering binding specificity. Although these mechanisms are distinct molecularly, both are predicted to act by enhancing SHP2 targeting to activated receptors or docking proteins and prolonging this interaction. In agreement with previously published data, this study provided evidence that the invariant NS-causing Y62D and Y63C amino acid substitutions perturb the stability of the N-SH2/PTP interaction required to maintain SHP2 in its catalytically inactive conformation. MD analyses, however, unexpectedly indicated that such a perturbing effect did not result from a local, direct consequence of the introduced residues, as observed previously for disease-causing mutations affecting codons 72 and 76 (9, 37), but instead from a more complex conformational rearrangement of the whole N-SH2 domain. Specifically, mutations A72V and E76K were

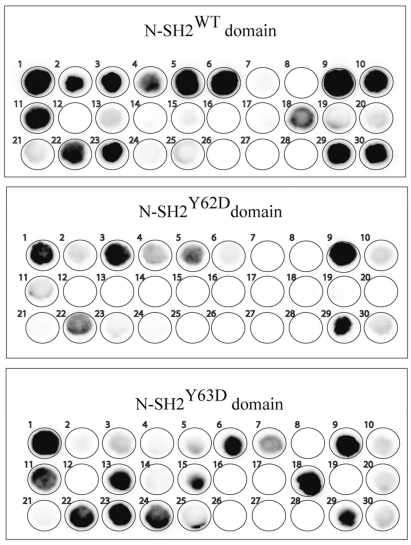

1:	Positive control of N-SH2 WT	M D E E L H y A S L N F H
2:	Positive control of N-SH2 WT	C E E E F K y A M L A L N
3:	Positive control of N-SH2 WT	E D R F I Q y A N P A F E
4:	Positive control of N-SH2 WT	N S C S L H y I N P Y Q P
5:	Positive control of N-SH2 WT	M E G L L H y I N P A H A
6:	Positive control of N-SH2 WT	T G K S G A y L I P L L E
7:	Inferred negative control for both domains	S T W F E A y E D K P P R
8:	Inferred negative control for both domains	R S T Y H G y R D D K G M
9:	SHP-2 peptide activator (SHPS1) -N Term	G G G D I T y A D L N L P
10:	SHP-2 peptide activator (SHPS1) -C Term	P N N H T E y A S I Q T S
11:	Inferred positive binders of Y63D	L F N L S T y L I P R H W
12:	Inferred negative binders of Y63D	S K C C C I y E K P R A F
13:	Inferred positive binders of Y63D	L A V M G A y V L L K R E
14:	Inferred negative binders of Y63D	V M L G A S y W Y R A R L
15:	Inferred positive binders of Y63D	F I R V V M y E G K K I M
16:	Inferred negative binders of Y63D	G C P E K V Y E L M R A C
17:	Tyrosine of GAB1 Y48	P D V L E Y y K N D H A K
18:	Tyrosine of GAB1 Y183	Q E D P Q D y L L L I N C
19:	Tyrosine of GAB1 Y242	F Q Q Q M I y D S P P S R
20:	Tyrosine of GAB1 Y259	S V D S S L y N L P R S Y
21:	Tyrosine of GAB1 Y285	E A D G E L y V F N T P S
22:	Tyrosine of GAB1 Y307	R H V S I S y D I P P T P
23:	Tyrosine of GAB1 Y317	P T P G N T y Q I P R T F
24:	Tyrosine of GAB1 Y373	S D T D S S y C I P T A G
25:	Tyrosine of GAB1 Y406	A S S Q D C y D I P R A F
26:	Tyrosine of GAB1 Y447	E E L D E N y V P M N P N
27:	Tyrosine of GAB1 Y472	P I Q E A N y V P M T P G
28:	Tyrosine of GAB1 Y589	H D S E E N y V P M N P N
29:	Tyrosine of GAB1 Y627	G D K Q V E y L D L D L D
30:	Tyrosine of GAB1 Y659	A D E R V D y V V V D Q Q

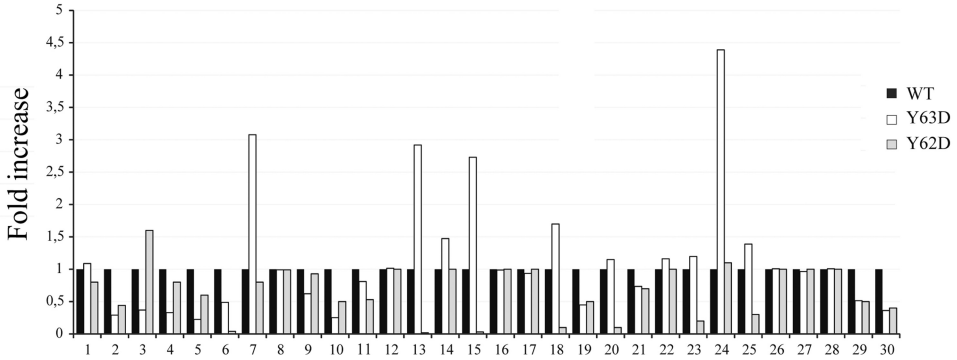

FIGURE 7. **Phosphopeptide recognition specificity in SPOT synthesis assay.** Phosphopeptides were synthesized on a cellulose membrane, which was incubated with the indicated N-SH2 domain expressed as a GST fusion protein. The binding efficiency and affinity were revealed using an anti-GST antibody conjugated to a fluorophore. The intensity of the signal was quantified, and the -fold increase (assuming the wild-type intensity equal to 1 for each peptide) was plotted in the bar chart.

shown to determine a direct destabilization of the N-SH2/PTP interface by introducing interdomain steric clashes (A72V) or electrostatic repulsion (E76K) (37). The structural consequences of amino acid substitutions affecting codons 62 and 63 are different. The Y63C change introduces a cavity in the intradomain hydrophobic core involving residues Phe^{41}, Ile^{56}, Cys^{63}, Leu^{65}, Phe^{71}, Ala^{72}, Leu^{74} and Leu^{77}. As a consequence, the N-SH2 blocking loop, which is inserted in the PTP catalytic cleft in the autoinhibited conformation of SHP2, undergoes a conformational transition that is predicted to perturb interdomain interactions. A similar effect was observed in the Y62D mutant. In this case, however, the driving force is the perturbation of the pattern of intradomain electrostatic interactions stabilizing the conformation of the blocking loop involving residues Asp^{61}, Asp^{62}, Asp^{64}, and Lys^{70}. A general rearrangement of the whole domain is also suggested for the Y63D mutant, for which fluctuations in the domain structure, including the residues constituting the N-SH2-binding site and the domain core, were observed. In both cases, possible effects on the N-SH2 binding competence were hypothesized because this region is also critical for the conformational transition leading to opening of the phosphopeptide-binding cleft (44). Consistent with these predictions, *in vitro* phosphatase and phosphopeptide binding analyses documented that a number of substitutions at codons 62 and 63 significantly perturb proper phosphopeptide binding efficiency and/or specificity. Such an effect dramatically occurred in the Y63D mutant and, to a lesser extent, in the NS-causing mutant protein carrying the Y62D substitution.

Multiple lines of evidence indicate that *PTPN11* mutations occurring as a somatic defect in hematologic malignancies have a greater gain-of-function effect than NS-causative lesions (5). The present study provides data indicating that, at least for a subset of germline defects, the weaker hyperactive behavior results from a less efficient functional up-regulation of the protein, in which two counteracting effects (*i.e.* destabilization of the inactive state and perturbed phosphopeptide binding properties) occur. Consistent with this model, structural and biochemical characterization of a large panel of germline *KRAS* mutations has documented that the milder hypermorphic effect promoted by these lesions, when compared with that induced by the oncogenic ones, results from a less effective capability of interacting with downstream effectors, as proved by the inability of these proteins to bind RAF1-RAS binding domain (RBD) or RALGDS-RBD efficiently (45). A similar observation has been reported for a recently identified HRAS mutant, $HRAS^{dupGlu37}$, associated with Costello syndrome (46),

a disorder clinically related to NS. This lesion affects the switch I region of the RAS effector loop, which is required for the interaction with a number of HRAS-binding partners, including GTPase-activating proteins (GAPs), guanine nucleotide exchange factors (GEFs), and effectors. It has been shown that the slightly enhanced signal flow through the MAPK and PI3K cascades promoted by this allele results from a counteracting effect between GTPase-activating protein insensitivity and inefficient binding to effector proteins, including RAF1. Of note, the finding that *PTPN11* mutations at codons 62 and 63 acting by destabilizing the autoinhibited SHP2 state but also severely affecting proper activation of the phosphatase after stimulation are not observed in the context of NS (or malignancy) documents the requirement for preserved phosphopeptide binding properties for SHP2 function and its functional up-regulation. This conclusion is in line with the absence of any developmental defect in mice heterozygous for a Shp2 mutant lacking the majority of the N-SH2 domain, $Shp2^{\Delta 46-110}$, which was demonstrated to be characterized by constitutive enhanced catalytic activity and inability to bind to intracellular signaling partners (47, 48).

In conclusion, our findings document that selection-by-function acts as a primary driving force for the largely invariant occurrence of NS-causing mutations involving codons 62 and 63 of SHP2. Our data indicate that missense single-base changes at those codons have a profound and complex effect on the functional regulation of SHP2 both by affecting the stability of the autoinhibitory interaction between the N-SH2 and PTP domains, but also by perturbing the structure and function of the pY-binding cleft. Among these mutations, the recurrent and largely invariant amino acid changes underlying NS are the only substitutions that significantly affect the catalytically inactive conformation of SHP2 without dramatically perturbing proper binding of the phosphatase to its phosphorylated signaling partners.

Acknowledgments—We are indebted to the Enrico Fermi Center for Study and Research and Interuniversity Consortium for the Application of Supercomputing for Universities and Research (CASPUR) (Rome, Italy) for providing computational resources.

REFERENCES

1. Tartaglia, M., Mehler, E. L., Goldberg, R., Zampino, G., Brunner, H. G., Kremer, H., van der Burgt, I., Crosby, A. H., Ion, A., Jeffery, S., Kalidas, K., Patton, M. A., Kucherlapati, R. S., and Gelb, B. D. (2001) Mutations in PTPN11, encoding the protein-tyrosine phosphatase SHP-2, cause Noonan syndrome. *Nat. Genet.* **29,** 465–468
2. Tartaglia, M., Gelb, B. D., and Zenker, M. (2011) Noonan syndrome and clinically related disorders. *Best Pract. Res. Clin. Endocrinol. Metab.* **25,** 161–179
3. Allanson, J. E. (2007) Noonan syndrome. *Am. J. Med. Genet. C Semin. Med. Genet.* **145C,** 274–279
4. van der Burgt, I. (2007) Noonan syndrome. *Orphanet J. Rare Dis.* **2,** 4
5. Tartaglia, M., and Gelb, B. D. (2010) Disorders of dysregulated signal traffic through the RAS-MAPK pathway: phenotypic spectrum and molecular mechanisms. *Ann. N.Y. Acad. Sci.* **1214,** 99–121
6. Neel, B. G., Gu, H., and Pao, L. (2003) The 'Shp'ing news: SH2 domain-containing tyrosine phosphatases in cell signaling. *Trends Biochem. Sci.* **28,** 284–293
7. Hof, P., Pluskey, S., Dhe-Paganon, S., Eck, M. J., and Shoelson, S. E. (1998) Crystal structure of the tyrosine phosphatase SHP-2. *Cell* **92,** 441–450
8. Tartaglia, M., Kalidas, K., Shaw, A., Song, X., Musat, D. L., van der Burgt, I., Brunner, H. G., Bertola, D. R., Crosby, A., Ion, A., Kucherlapati, R. S., Jeffery, S., Patton, M. A., and Gelb, B. D. (2002) PTPN11 mutations in Noonan syndrome: molecular spectrum, genotype-phenotype correlation, and phenotypic heterogeneity. *Am. J. Hum. Genet.* **70,** 1555–1563
9. Tartaglia, M., Martinelli, S., Stella, L., Bocchinfuso, G., Flex, E., Cordeddu, V., Zampino, G., Burgt, I., Palleschi, A., Petrucci, T. C., Sorcini, M., Schoch, C., Foa, R., Emanuel, P. D., and Gelb, B. D. (2006) Diversity and functional consequences of germline and somatic PTPN11 mutations in human disease. *Am. J. Hum. Genet.* **78,** 279–290
10. Keilhack, H., David, F. S., McGregor, M., Cantley, L. C., and Neel, B. G. (2005) Diverse biochemical properties of Shp2 mutants: implications for disease phenotypes. *J. Biol. Chem.* **280,** 30984–30993
11. Martinelli, S., Torreri, P., Tinti, M., Stella, L., Bocchinfuso, G., Flex, E., Grottesi, A., Ceccarini, M., Palleschi, A., Cesareni, G., Castagnoli, L., Petrucci, T. C., Gelb, B. D., and Tartaglia, M. (2008) Diverse driving forces underlie the invariant occurrence of the T42A, E139D, I282V, and T468M SHP2 amino acid substitutions causing Noonan and LEOPARD syndromes. *Hum. Mol. Genet.* **17,** 2018–2029
12. Sarkozy, A., Digilio, M. C., and Dallapiccola, B. (2008) Leopard syndrome. *Orphanet J. Rare Dis.* **3,** 13
13. Hanna, N., Montagner, A., Lee, W. H., Miteva, M., Vidal, M., Vidaud, M., Parfait, B., and Raynal, P. (2006) Reduced phosphatase activity of SHP-2 in LEOPARD syndrome: consequences for PI3K binding on Gab1. *FEBS Lett.* **580,** 2477–2482
14. Kontaridis, M. I., Swanson, K. D., David, F. S., Barford, D., and Neel, B. G. (2006) PTPN11 (Shp2) mutations in LEOPARD syndrome have dominant negative, not activating, effects. *J. Biol. Chem.* **281,** 6785–6792
15. Tartaglia, M., Niemeyer, C. M., Fragale, A., Song, X., Buechner, J., Jung, A., Hählen, K., Hasle, H., Licht, J. D., and Gelb, B. D. (2003) Somatic mutations in PTPN11 in juvenile myelomonocytic leukemia, myelodysplastic syndromes, and acute myeloid leukemia. *Nat. Genet.* **34,** 148–150
16. Tartaglia, M., Martinelli, S., Cazzaniga, G., Cordeddu, V., Iavarone, I., Spinelli, M., Palmi, C., Carta, C., Pession, A., Aricò, M., Masera, G., Basso, G., Sorcini, M., Gelb, B. D., and Biondi, A. (2004) Genetic evidence for lineage-related and differentiation stage-related contribution of somatic PTPN11 mutations to leukemogenesis in childhood acute leukemia. *Blood* **104,** 307–313
17. Tartaglia, M., Martinelli, S., Iavarone, I., Cazzaniga, G., Spinelli, M., Giarin, E., Petrangeli, V., Carta, C., Masetti, R., Aricò, M., Locatelli, F., Basso, G., Sorcini, M., Pession, A., and Biondi, A. (2005) Somatic PTPN11 mutations in childhood acute myeloid leukemia. *Br. J. Haematol.* **129,** 333–339
18. Chan, R. J., Leedy, M. B., Munugalavadla, V., Voorhorst, C. S., Li, Y., Yu, M., and Kapur, R. (2005) Human somatic PTPN11 mutations induce hematopoietic cell hypersensitivity to granulocyte-macrophage colony-stimulating factor. *Blood* **105,** 3737–3742
19. Schubbert, S., Lieuw, K., Rowe, S. L., Lee, C. M., Li, X., Loh, M. L., Clapp, D. W., and Shannon, K. M. (2005) Functional analysis of leukemia-associated PTPN11 mutations in primary hematopoietic cells. *Blood* **106,** 311–317
20. Fragale, A., Tartaglia, M., Wu, J., and Gelb, B. D. (2004) Noonan syndrome-associated SHP2/PTPN11 mutants cause EGF-dependent prolonged GAB1 binding and sustained ERK2/MAPK1 activation. *Hum. Mutat.* **23,** 267–277
21. Baker, N. A., Sept, D., Joseph, S., Holst, M. J., and McCammon, J. A. (2001) Electrostatics of nanosystems: application to microtubules and the ribosome. *Proc. Natl. Acad. Sci. U.S.A.* **98,** 10037–10041
22. Hess, B., Kutzner, C., van der Spoel, D., and Lindahl, E. (2008) GROMACS 4: algorithms for highly efficient, load-balanced, and scalable molecular simulation. *J. Chem. Theory Comput.* **4,** 435–447
23. van Gunsteren, W. F., Billeter, S. R., Eising, A. A., Hünenberger, P. H., Krüger, P., Mark, A. E., Scott, W. R. P., and Tironi, I. G. (1996) *Biomolecular Simulation: The GROMOS96 Manual and User Guide*, Hochschulverlag AG an der ETH Zurich Press, Zürich, Switzerland
24. Guex, N., and Peitsch, M. C. (1997) SWISS-MODEL and the Swiss-Pdb-Viewer: an environment for comparative protein modeling. *Electrophore-*

sis **18,** 2714–2723
25. Berendsen, H. J., Postma, J. P., van Gunsteren, W. F., and Hermans, J. (1981) *Interaction Models for Water in Relation to Protein Hydration* in *Intermolecular Forces* (Pullman, B., ed) pp. 331–342, Reidel Publishing Company, Dordrecht, The Netherlands
26. Miyamoto, S., and Kollman, P. A. (1992) Settle: an analytical version of the SHAKE and RATTLE algorithm for rigid water models. *J. Comp. Chem.* **13,** 952–962
27. Berendsen, H. J., Postma, J. P., van Gunsteren, W. F., Di Nola, A., and Haak, J. R. (1984) Molecular dynamics with coupling to an external bath. *J. Chem. Phys.* **81,** 3684–3690
28. Hess, B., Bekker, H., Berendsen, H. J., and Fraaije, J. G. (1997) LINCS: a linear constraint solver for molecular simulations. *J. Comp. Chem.* **18,** 1463–1472
29. Koradi, R., Billeter, M., and Wüthrich, K. (1996) MOLMOL: a program for display and analysis of macromolecular structures. *J. Mol. Graph.* **14,** 51–55
30. Pettersen, E. F., Goddard, T. D., Huang, C. C., Couch, G. S., Greenblatt, D. M., Meng, E. C., and Ferrin, T. E. (2004) UCSF Chimera: a visualization system for exploratory research and analysis. *J. Comput. Chem.* **25,** 1605–1612
31. Sacco, F., Tinti, M., Palma, A., Ferrari, E., Nardozza, A. P., Hooft van Huijsduijnen, R., Takahashi, T., Castagnoli, L., and Cesareni, G. (2009) Tumor suppressor density-enhanced phosphatase-1 (DEP-1) inhibits the RAS pathway by direct dephosphorylation of ERK1/2 kinases. *J. Biol. Chem.* **284,** 22048–22058
32. Diella, F., Cameron, S., Gemünd, C., Linding, R., Via, A., Kuster, B., Sicheritz-Pontén, T., Blom, N., and Gibson, T. J. (2004) Phospho.ELM: a database of experimentally verified phosphorylation sites in eukaryotic proteins. *BMC Bioinformatics* **5,** 79
33. Blom, N., Gammeltoft, S., and Brunak, S. (1999) Sequence and structure-based prediction of eukaryotic protein phosphorylation sites. *J. Mol. Biol.* **294,** 1351–1362
34. Vacic, V., Iakoucheva, L. M., and Radivojac, P. (2006) Two Sample Logo: a graphical representation of the differences between two sets of sequence alignments. *Bioinformatics* **22,** 1536–1537
35. Hilpert, K., Winkler, D. F., and Hancock, R. E. (2007) Peptide arrays on cellulose support: SPOT synthesis, a time- and cost-efficient method for synthesis of large numbers of peptides in a parallel and addressable fashion. *Nat. Protoc.* **2,** 1333–1349
36. O'Reilly, A. M., Pluskey, S., Shoelson, S. E., and Neel, B. G. (2000) Activated mutants of SHP-2 preferentially induce elongation of *Xenopus* animal caps. *Mol. Cell Biol.* **20,** 299–311
37. Bocchinfuso, G., Stella, L., Martinelli, S., Flex, E., Carta, C., Pantaleoni, F., Pispisa, B., Venanzi, M., Tartaglia, M., and Palleschi, A. (2007) Structural and functional effects of disease-causing amino acid substitutions affecting residues Ala^{72} and Glu^{76} of the protein-tyrosine phosphatase SHP-2. *Proteins* **66,** 963–974
38. Songyang, Z., Shoelson, S. E., Chaudhuri, M., Gish, G., Pawson, T., Haser, W. G., King, F., Roberts, T., Ratnofsky, S., Lechleider, R. J., *et al.* (1993) SH2 domains recognize specific phosphopeptide sequences. *Cell* **72,** 767–778
39. Qin, C., Wavreille, A. S., and Pei, D. (2005) Alternative mode of binding to phosphotyrosyl peptides by Src homology-2 domains. *Biochemistry* **44,** 12196–12202
40. Sweeney, M. C., Wavreille, A. S., Park, J., Butchar, J. P., Tridandapani, S., and Pei, D. (2005) Decoding protein-protein interactions through combinatorial chemistry: sequence specificity of SHP-1, SHP-2, and SHIP SH2 domains. *Biochemistry* **44,** 14932–14947
41. Lee, C. H., Kominos, D., Jacques, S., Margolis, B., Schlessinger, J., Shoelson, S. E., and Kuriyan, J. (1994) Crystal structures of peptide complexes of the amino-terminal SH2 domain of the Syp tyrosine phosphatase. *Structure* **2,** 423–438
42. Eck, M. J., Pluskey, S., Trüb, T., Harrison, S. C., and Shoelson, S. E. (1996) Spatial constraints on the recognition of phosphoproteins by the tandem SH2 domains of the phosphatase SH-PTP2. *Nature* **379,** 277–280
43. Dechert, U., Adam, M., Harder, K. W., Clark-Lewis, I., and Jirik, F. (1994) Characterization of protein-tyrosine phosphatase SH-PTP2: study of phosphopeptide substrates and possible regulatory role of SH2 domains. *J. Biol. Chem.* **269,** 5602–5611
44. Guvench, O., Qu, C. K., and MacKerell, A. D., Jr. (2007) Tyr^{66} acts as a conformational switch in the closed-to-open transition of the SHP-2 N-SH2 domain phosphotyrosine-peptide-binding cleft. *BMC Struct. Biol.* **7,** 14
45. Gremer, L., Merbitz-Zahradnik, T., Dvorsky, R., Cirstea, I. C., Kratz, C. P., Zenker, M., Wittinghofer, A., and Ahmadian, M. R. (2011) Germline KRAS mutations cause aberrant biochemical and physical properties leading to developmental disorders. *Hum. Mutat.* **32,** 33–43
46. Gremer, L., De Luca, A., Merbitz-Zahradnik, T., Dallapiccola, B., Morlot, S., Tartaglia, M., Kutsche, K., Ahmadian, M. R., and Rosenberger, G. (2010) Duplication of Glu^{37} in the switch I region of HRAS impairs effector/GAP binding and underlies Costello syndrome by promoting enhanced growth factor-dependent MAPK and AKT activation. *Hum. Mol. Genet.* **19,** 790–802
47. Qu, C. K., Shi, Z. Q., Shen, R., Tsai, F. Y., Orkin, S. H., and Feng, G. S. (1997) A deletion mutation in the SH2-N domain of Shp-2 severely suppresses hematopoietic cell development. *Mol. Cell. Biol.* **17,** 5499–5507
48. Saxton, T. M., Henkemeyer, M., Gasca, S., Shen, R., Rossi, D. J., Shalaby, F., Feng, G. S., and Pawson, T. (1997) Abnormal mesoderm patterning in mouse embryos mutant for the SH2 tyrosine phosphatase Shp-2. *EMBO J.* **16,** 2352–2364